







# Virtual Inertia Scheduling (VIS) for Microgrids with Static and Dynamic Security Constraints

Buxin She , *Member, IEEE*, Fangxing Li , *Fellow, IEEE*, Jinning Wang , *Graduate Student Member, IEEE*, Hantao Cui , *Senior Member, IEEE*, Xiaofei Wang , *Member, IEEE*, Rui Bo , *Senior Member, IEEE*

**Abstract**—Microgrids feature a high penetration of inverter-interfaced distributed energy resources (DERs). The low inertia characteristic and fast dynamics of DERs pose challenges to conventional decoupled static economic operation and dynamic control design within microgrids. Hence, this paper proposed virtual inertia scheduling (VIS) for microgrids, aiming to ensure both economy and security. First, a unified framework for device-level control and grid-level operation is introduced, with VIS serving as a key application to address low inertia issues. VIS actively harnesses the controllability and flexibility of DERs to effectively manage microgrid inertia. It updates the conventional economic operation framework by incorporating the virtual inertia/damping cost, transient performance constraints, and stability constraints. Control parameters for DERs are formulated as additional decision variables. Then, VIS is specified in microgrids, followed by explication and linearization of dynamic constraints. An efficient workflow is developed to facilitate the integration of data-driven methods into microgrid-VIS, involving data generation, cleaning, and labeling to alleviate computational burdens. Time-domain simulations are further integrated for correction, validation, and performance guarantee. Finally, VIS is verified in an islanded microgrid modified from the IEEE 123-bus system. Results demonstrate that VIS effectively addresses the low inertia challenges in DER-penetrated microgrids, balancing economic considerations and dynamic performance.

**Index Terms**—Economic dispatch, virtual inertia scheduling (VIS), stability constraints, microgrid, distributed energy resource (DER).

## NOMENCLATURE

$a^{sg}, a^{ibr}$	Quadratic cost of synchronous generators (SGs) and inverter-based resources (IBRs).
$a_{m[n]}$	ReLU's activation status of $n$ th neuron at the $m$ th hidden layer.
$b^{sg}, b^{ibr}$	Linear cost of SGs and IBRs.
$c^{sg}, c^{ibr}$	Constant generation cost of SGs and IBRs.
$C_t^{aux}$	Auxiliary service cost at time $t$ .
$C_t^{gen}$	Generation cost at time $t$ .
$d$	Linear inertia cost.
$D$	Damping coefficient.
$D_{i,t}^{ibr}$	Virtual damping of IBR $i$ at time $t$ .
$\overline{D}_i^{ibr}, \underline{D}_i^{ibr}$	Lower and upper damping limit of IBR $i$ .
$e$	Linear damping cost.
$eig_{\max,i}^{real}$	Maximum real part of eigenvalue.

$\Omega^G$	Generator set.
$h$	Large enough constant.
$(i, j)$	Branch $(i, j)$ .
$I_{ij}$	Branch current.
$M$	Moment of inertia.
$M_{i,t}^{ibr}$	Virtual inertia of IBR $i$ at time $t$ .
$P_{i,t}^{sg}, P_{i,t}^{ibr}$	Power output of SG $i$ and IBR $i$ at time $t$ .
$P_{ij}, Q_{ij}$	Branch active and reactive power.
$p_i, q_i$	Node active and reactive power.
$r_{ij}$	Branch resistance.
$RoCoF$	Rate of change of frequency.
$\overline{RoCoF}$	Upper $RoCoF$ limit.
$\underline{RoCoF}$	Lower $RoCoF$ limit.
$S_{ij}$	Apparent power.
$t$	Time.
$T$	Total scheduling interval.
$V_i$	Voltage at node $i$ .
$v_i$	The square of the voltage amplitude.
$x_{ij}$	Branch reactance.
$\Delta f_{nadir}$	Frequency nadir deviation.
$\Delta f, \overline{\Delta f}$	Lower and upper limit of frequency deviation.
$\overline{\Delta \delta}_{\max}$	Maximum power angle difference.
$\hat{z}_{m[n]}$	Linear output of $n$ th neuron at the $m$ th hidden layer.
$z_{m[n]}$	Activation function output of $n$ th neuron at the $m$ th hidden layer.
$\delta_j(t)$	Power angle of generator $j$ at time $t$ .
$\Delta \delta_{\max}$	Maximum power angle difference.
$\mathcal{B}$	Branch set.
$\mathcal{N}$	Node set.
$\Theta$	Decision variable set.
$\Theta^{ss}$	Decision variable set that ensures small-signal stability.
$\Theta^{ls}$	Decision variable set that ensures large-signal stability.
$\Psi$	Contingency set
$\Psi_t$	Contingency at time $t$ .

## I. INTRODUCTION

Positioned as an essential infrastructure component in future power systems, microgrids are gaining increased attention for their advantages [1], including various renewable energy accommodations, efficient energy management, and enhanced resilience. Facilitated by the integration of distributed energy resources (DERs) interfaced with inverters, known as inverter-based resources (IBRs), microgrids exhibit the

B. She, F. Li, J. Wang, and X. Wang are with the Department of Electrical Engineering and Computer Science, The University of Tennessee, Knoxville, TN 37996, USA.

H. Cui is with the Department of Electrical and Computer Engineering, North Carolina State University, Raleigh, NC 27695, USA.

R. Bo is with the Department of Electrical and Computer Engineering, Missouri University of Science and Technology, Rolla, MO 65409, USA.

flexibility to operate either in grid-connected mode, providing grid support, or in islanded mode, forming a local and self-sufficient system [2], [3].

Despite the benefits brought by IBRs, they pose certain challenges to the operation and control of microgrids. The fast dynamics inherent in IBRs impact the conventional static economic operation and degrade the stability of power electronic interfaced systems. Specifically, IBRs can change the nature of unstable modes and underlying dynamics, potentially challenging the optimal power flow (OPF) result [4]. Furthermore, in comparison to conventional synchronous generators (SGs), IBRs have lower overload capability and short circuit ratio, rendering them more vulnerable to disturbances. More importantly, they have insufficient physical inertia and thus reduce the overall inertia of the microgrid.

Low physical inertia increases the rate of change of frequency (RoCoF) to excessive levels and lowers the frequency nadir. It may energize the protection relays of load-shedding and potentially result in generation trips and successive outages [5]. Hence, there is a lot of work addressing the low-inertia issues of microgrids. They are categorized into three aspects as follows.

1) *Emulating inertia through virtual synchronous generator (VSG) control*: The first group of work focuses on the device-level inertia emulation of IBRs. They draw inertia support from IBRs by developing advanced VSG control algorithms. VSG-controlled IBRs can provide virtual inertia support by rapidly increasing the active power injection after a disturbance under the guidance of pre-configured control strategies. Grid-following IBRs are controlled as current sources, with power references updated based on microgrid frequency deviations. Grid-forming IBRs, acting as voltage sources, are controlled based on the swing equation derived from SGs.

Basic VSG is enhanced through adaptive control, model-predictive control (MPC), and data-driven control to make IBRs more efficiently adapt to the change of microgrid inertia and frequency [6]–[10]. For example, [6] proposes an adaptive VSG control for microgrids based on constrained MPC, aimed at minimizing frequency deviation and control efforts. Ref. [7] proposes an adaptive VSG to address the conflict between the transient response of the active power and the angle frequency. Notably, the angular frequency stability needs a larger inertia, while the active power response leans towards a smaller inertia. Moreover, [8] proposes an improved VSG control algorithm to address the contradiction between steady-state deviation in active power and dynamic impact regulation. This is achieved by cascading a differential into the first-order virtual inertia forward channel. Additional approaches utilizing MPC for VSG control in frequency regulation are detailed in [9], [10].

Despite the sophistication of these advanced VSG control algorithms, they are typically implemented locally without system-level coordination. The absence of such coordination can lead to increased costs, as inertia support through VSG control is not free. Extra headroom is often offset from the maximum power point tracking (MPPT) [11], or auxiliary battery energy storage systems (BESS) are required during inertia support [12].

2) *Developing security-constrained economic operation*: The second group of work focuses on system-level security-constrained economic operation, integrating dynamic constraints—such as the transient performance quantified by frequency nadir, RoCoF, and settling time [13]—and stability constraints like small-signal stability criteria and transient stability constraints [14] into the conventional static OPF.

Ref. [15] introduces a probabilistic transient stability-constrained OPF method, integrating the critical clearing time and instability mode. Ref. [4] incorporates small-signal stability constraints into OPF using a Lyapunov stability equation. A convex relaxation method combining semidefinite programming, parabolic relaxations, and sequential heuristic penalty function is developed to solve the problem. In [16], the frequency divider formula (discretized model) is employed to predict RoCoF and angle difference explicitly based on local variables, subsequently integrated into OPF to ensure transient stability. Additionally, [17] integrates the voltage stability constraints into microgrid OPF in the presence of plug-in electric vehicles. Ref. [18] actively designs control parameters of IBRs, integrating the small signal stability constraints into OPF and solving it with particle swarm optimization (PSO). In [19], a bilinear matrix inequality method based on Semidefinite Programming (SDP) is developed to ensure small signal stability for OPF problems. A vector-norm-based objective penalty function is also proposed for feasibility recovery while working over large and dense binary matrix variables.

While the second group of efforts addresses the dynamic challenges at the system level, IBRs are typically viewed as passive devices providing limited virtual inertia, without leveraging their flexibility and controllability [4], [15]–[17], [19]. Furthermore, they usually focus on a single type of dynamic constraint. A unified framework that integrates diverse dynamic constraints, particularly those arising after large disturbances, has yet to be developed.

3) *Pioneering the inertia market*: The third group work focuses on the development of an inertia market to incentivize both the generation and demand side owner to contribute to grid-level inertia support. Unlike the conventional auxiliary market, the inertia market has not yet been well-established in America. Ref. [20] proposes an inertia market mechanism for virtual inertia, where the system dynamics are approximated by a linearized state space model. A robust  $H_2$  performance metric penalizes the worst-case primary control effort. As for industry efforts, initiatives such as the Enhanced Frequency Control Capability (EFCC) project and Future Power System Security Program project are established by the National Grid and Australia Energy Market Operator, respectively [21]. However, these market-related works focus on inertia support from an economic perspective, overlooking the dynamic constraints and active control of IBRs.

Based on the above discussion, it is critical to develop an inertia management framework that considers both the static economic operation and dynamic control of IBRs in microgrids. Hence, this paper extends the concept of virtual inertia scheduling (VIS), initially proposed in [22], and adapts it to microgrid applications. Although VIS has been introduced, two main gaps remain to be addressed. First, the

transient performance constraints are derived from a linear uniform frequency dynamics model under the assumption of regular disturbances. This linear model is less accurate compared to full-order simulation-based approaches, particularly under conditions of large disturbances. Second, stability considerations, which are crucial when device-level parameter tuning is integrated into system-level operations, were not addressed. Most existing planning and operational strategies, including those in [22], ignore these stability constraints, which is increasingly critical given the rising frequency of larger disturbances under extreme events [23].

This paper addresses these gaps by incorporating dynamic constraints, including transient performance and small- and large-signal stability constraints, within a contingency set that accounts for large disturbances. A unified framework, along with its generic mathematical formulation for unified device-level control and grid-level operation, is proposed. It is exemplified in microgrid-VIS to address low-inertia and stability issues. The proposed formulation seamlessly integrates key static economic operation constraints, dynamic stability considerations, and performance metrics, ensuring that microgrids operate within both static and dynamic security contexts. The contributions of this paper are outlined as follows:

- Elaboration of a unified device-level control and grid-level operation framework, along with the development of a generic mathematical formulation that enables customization of the scheduling interval, decision set, and both static and dynamic constraints.
- Configuration of microgrid-VIS for operation problem with a particular focus on ensuring stability after both small and large disturbances, achieved through the integration of data-driven dynamic approximation.
- Enhancement of data-driven approaches to seamlessly incorporate dynamic approximations into the dispatch problem, including efficient batch data generation, innovative cleaning and labeling of unusual data, and time-domain simulation (TDS)-based correction and validation.

The rest of this paper is organized as follows. Section II introduces a unified control and operation framework and its generic mathematical formulation. Section III exemplifies VIS in microgrids with static and dynamic security constraints, followed by linearization approaches. Section IV introduces the data-driven workflow that includes batch data generation, cleaning, labeling, and TDS-based correction and validation. Case studies are conducted in Section V, followed by conclusions drawn in Section VI.

## II. UNIFIED DEVICE-LEVEL CONTROL AND GRID-LEVEL OPERATION: CONCEPT AND GENERIC FORMULATION

This section explores the evolving role of IBRs in microgrids. It also introduces the unified framework for device-level control and grid-level operation, designed to adapt to these changes and optimize grid stability and performance.

### A. Unified Device-level Control and Grid-level Operation

1) *IBR Role Transition from Passive to Active Participants*: Microgrids dominated by IBRs face distinct challenges,

including uncertainty, low inertia, and voltage fluctuations, all of which can threaten microgrid stability. To address these challenges, it is essential to transition IBRs from passive components to active participants in microgrid management. As shown in Fig. 1, IBRs can be enhanced with advanced control capabilities that not only optimize their operations but also actively contribute to grid security by providing critical services such as inertia emulation and damping support. This transition marks a significant shift in how IBRs are managed within microgrids, evolving from a reactive role to one that actively shapes their characteristics and overall grid dynamics.

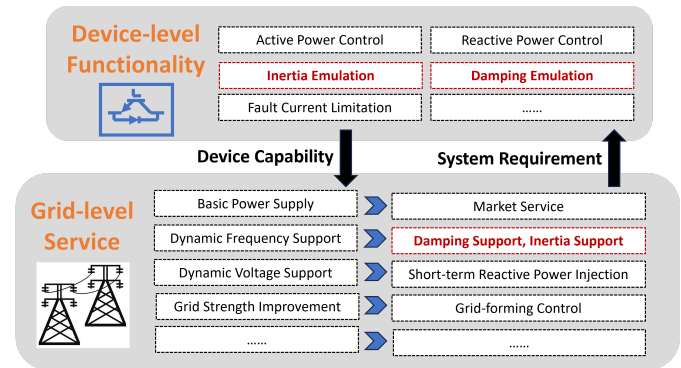


Fig. 1. The role of IBRs in microgrids.

2) *Unified Framework Overview*: The transition of IBRs into active grid components necessitates a unified framework that integrates device-level control with grid-level operations. This framework leverages the inherent controllability and flexibility of IBRs—devices driven by controllers, as opposed to traditional SGs, which are governed by physical laws. In this unified approach, IBRs’ external characteristics must be carefully considered and actively optimized at the system level to deliver essential grid services. As visualized in Fig. 1, these services range from basic power supply and dynamic frequency support to advanced market services like damping and inertia support.

This unified framework ensures that the control of IBRs at the device level is optimized to meet the grid-level requirements, effectively balancing economic efficiency with dynamic performance. By coordinating both device-level functionalities—such as active and reactive power control, inertia emulation, and damping emulation—and grid-level services, this framework enables IBRs to play a crucial role in maintaining microgrid stability and reliability.

### B. Generic Mathematical Formulation

The unified framework motivates a comprehensive mathematical formulation to determine the control and operational variables for microgrids. Eq. (1) shows the generic compact model of the unified device-level control and grid-level operation framework. It is formulated as an optimization problem, aiming to achieve an economic objective function while satisfying physical constraints.

$$\begin{aligned} & \min_{\Theta} \sum_{t \in T} C_t^{gen} + C_t^{aux} \\ & \text{For } \forall t = 1, 2, \dots, T \text{ and } \psi_t \in \Psi, \\ & \text{s.t. } \begin{cases} \text{i). Economic dispatch constraints} \\ \text{ii). Transient performance constraints} \\ \text{iii). Stability constraints} \end{cases} \end{aligned} \quad (1)$$

The generic mathematical formulation of the unified control and operation framework exhibits several distinct features compared to the conventional economic dispatch model.

- Incorporation of auxiliary service cost in the objective function. The increasing penetration of renewable energy interfaced by inverters degrades the strength of power grids, consequently increasing the expenses associated with system maintenance. Considering these costs, such as the virtual inertia and damping support cost [20], is important in the ongoing development of auxiliary service markets.
- Formulate the device-level control parameters as decision variables for grid components to provide better active support. The decision variable set includes not only the conventional economic dispatch variables but also control variables that determine the dynamic support capability of grid components. Higher support capability typically involves increased control efforts or cost, necessitating customized design and coordination.
- Integration of the transient performance constraints. Conventional economic operations usually consider static constraints, such as power flow constraints, generation constraints, line thermal limit constraints, and voltage constraints. These indices quantify the grid's state transition performance between equilibrium. It is crucial to keep them within specific bounds to prevent the activation of protection relays, which could lead to load shedding or generation trips [5], [24].
- Integration of the stability constraints, covering small- and large-signal stability constraints. They quantify the ability of a power grid, for a given initial operating condition, to regain a state of operating equilibrium after being subjected to a physical disturbance, with most system variables bounded so that practically the entire system remains intact [25]. As the control variables are actively designed at the device level and can fundamentally impact grid stability, it is necessary to incorporate these constraints for stability guarantee.
- Facilitation of flexible modeling for diverse application scenarios. It can either be a single-interval or multi-interval optimization by adjusting the scheduling interval  $T$ . Also, the decision variable set can be custom-designed, and the contingency set can include extreme events to enhance the resilience of microgrids.

In summary, the generalized formulation presented in (1) facilitates microgrid operation with adaptable static and dynamic security constraints. This formulation is particularly effective in addressing the low-inertia and frequency-related challenges arising from the increasing integration of IBRs, as discussed in Section III.

### III. MICROGRID VIRTUAL INERTIA SCHEDULING WITH STATIC AND DYNAMIC SECURITY CONSTRAINTS

Building on the unified control and operation framework, this section formulates microgrid-VIS for the inertia management of microgrids with static and dynamic security constraints. Linearization approaches are introduced to facilitate the solution of the nonlinear model.

#### A. Concept of VIS

VIS is a typical unified device-level control and grid-level operation method, with a focus on low-inertia issues in power grids penetrated by IBRs. It actively manages grid components to provide secure and economic damping and inertia support.

Grid components can provide passive inertia support or actively change their operation modes to provide active (virtual) inertial support. For example, motor loads contribute passive inertia support like SGs by releasing stored energy in rotating mass. IBRs, on the other hand, can emulate SGs through elaborate control algorithm design, actively providing virtual inertia support. To have a good dynamic performance, the straightforward approach is to have each grid component operate in its maximum inertia support mode. However, active inertia support is not free. The energy for inertia support generally comes from the extra headroom of PV or BESS [26], introducing additional opportunity costs or investments. Hence, it is essential to strike a balance between dynamic performance and economic considerations, thereby motivating the proposal of microgrid-VIS.

#### B. Formulation of microgrid-VIS

Eqs. (2)-(8) formulate microgrid-VIS by specifying the objective function, decision variables, scheduling interval, contingency set, and constraints in (1).

$$\min_{\Theta} \sum_{t \in T} C_t^{gen} + C_t^{aux} \quad (2)$$

$$C_t^{gen} = \sum_{t \in T} \underbrace{\sum_{sg}^{N_{sg}=1} (a_{i,t}^{sg} P_{i,t}^{sg2} + b_{i,t}^{sg} P_{i,t}^{sg} + c_{i,t}^{sg})}_{SG} \quad (3)$$

$$+ \underbrace{\sum_{i=1}^{N_{ibr}} (a_{i,t}^{ibr} P_{i,t}^{ibr2} + b_{i,t}^{ibr} P_{i,t}^{ibr} + c_{i,t}^{ibr})}_{IBR}$$

$$C_t^{aux} = \sum_{t \in T} \sum_{i=1}^{N_{ibr}} d_{i,t}^{ibr} M_{i,t}^{ibr} + e_{i,t}^{ibr} D_{i,t}^{ibr} \quad (4)$$

$$\Theta \triangleq [P_{ij}, Q_{ij}, v_i, p_i, q_i, M, D] \quad (5)$$

$$i). \begin{cases} V_i - V_j = z_{ij} I_{ij}, \forall (i, j) \in \mathcal{B} \\ S_{ij} = V_i I_{ij}^*, \forall (i, j) \in \mathcal{B} \\ \sum_{k:j \rightarrow k} S_{jk} - \sum_{i:i \rightarrow j} S_{ij} \\ (S_{ij} - z_{ij} |I_{ij}|^2) = s_j, \forall j \in \mathcal{N} \\ \underline{V}_i \leq V_i \leq \overline{V}_i, \forall i \in \mathcal{N} \\ \underline{s}_i^g \leq s_i^g \leq \overline{s}_i^g, \forall i \in \mathcal{N} \\ \underline{I}_{ij} \leq I_{ij} \leq \overline{I}_{ij}, \forall (i, j) \in \mathcal{B} \end{cases} \quad (6)$$

$$ii). \begin{cases} \frac{M_i^{ibr}}{D_i^{ibr}} \leq M_i^{ibr} \leq \overline{M_i^{ibr}}, \forall i \in \mathcal{R} \\ D_i^{ibr} \leq D_i^{ibr} \leq \overline{D_i^{ibr}}, \forall i \in \mathcal{R} \\ \underline{RoCoF} \leq RoCoF \leq \overline{RoCoF} \\ \underline{\Delta f} \leq \Delta f \leq \overline{\Delta f} \end{cases} \quad (7)$$

$$iii). \begin{cases} \Theta \in \Theta^{ss} \\ \Theta \in \Theta^{ls} \end{cases} \quad (8)$$

Microgrid-VIS is formulated as an optimization problem with the objective of minimizing the quadratic generation cost in (3) and linear inertia and damping support cost in (4). Considering that IBRs are among the most controllable and flexible active components that can provide inertia support, the virtual inertia and damping of VSG-controlled IBRs are formulated as decision variables in (5). Eq. (6) is nonlinear distribution power flow constraints, (7) is transient performance constraint, and (8) is stability constraints covering both small- and large-signal stability constraints. The contingency set includes both normal load change and unplanned generation trips.

### C. Linearization of microgrid-VIS

While (2)-(8) formulate microgrid-VIS with static and dynamic security constraints following load change and generation trips, they are non-linear, non-convex, and implicit models. Hence, this subsection aims to linearize distribution power flow constraints and make (7)-(8) explicit.

1) *Linearized distribution power flow*: Referring to the assumptions in [27], [28], the nonlinear terms in (6) can be ignored since they are much smaller than the linear branch flow terms. In addition, assuming the bus voltage is close to the nominal value, then nonlinear distribution power flow can be simplified as follows.

$$i). \begin{cases} p_j = \sum_{k:j \rightarrow k} P_{jk} - \sum_{i:i \rightarrow j} P_{ij}, \forall j \in \mathcal{N} \\ q_j = \sum_{k:j \rightarrow k} Q_{jk} - \sum_{i:i \rightarrow j} Q_{ij}, \forall j \in \mathcal{N} \\ v_j = v_i - (r_{ij}P_{ij} + x_{ij}Q_{ij}), \forall (i, j) \in \mathcal{B} \\ \underline{v}_i \leq |v_i| \leq \overline{v}_i, \forall i \in \mathcal{N} \\ \underline{p}_i^g \leq |p_i^g| \leq \overline{p}_i^g, \forall i \in \mathcal{N} \\ \underline{q}_i^g \leq |q_i^g| \leq \overline{q}_i^g, \forall i \in \mathcal{N} \end{cases} \quad (9)$$

2) *Linearized stability constraints and transient performance index*: There are generally two types of methods to make (7)-(8) explicit: model-based methods and data-driven methods. Model-based methods derive the transient performance index and stability criteria based on the system model [14]. However, most indexes are derived under normal operation conditions, and the corresponding criteria are for ensuring small-signal stability [4], [29]. Deriving an analytical large-signal stability criterion is challenging [30]. Furthermore, these derived indices and criteria may not be inherently convex and accurate after derivation, making it difficult to seamlessly integrate into microgrid-VIS.

The data-driven methods, on the other hand, are flexible and can be customized to cover various scenarios and capture highly nonlinear relationships. Inspired by [31], [32], this paper predicts both transient performance indices and stability with DNNs and integrates them into VIS. As shown in (10), a DNN with the ReLU activation function maps the decision variables and contingencies to RoCoF, frequency nadir, and

the stability condition. Then, (10) can be linearized and incorporated into microgrid-VIS based on (11), transforming (1) into a mix-integer linear programming problem (MILP) [33].

$$RoCoF, \Delta f_{\text{nadir}}, \Theta^{ss}, \Theta^{ls} = DNN(\Theta, \psi) \quad (10)$$

$$\begin{cases} z_{m[n]} \leq \hat{z}_{m[n]} + h * (1 - a_{m[n]}) \\ z_{m[n]} \geq \hat{z}_{m[n]} \\ z_{m[n]} \leq h * a_{m[n]} \\ z_{m[n]} \geq 0 \\ a_{m[n]} \in \{0, 1\} \end{cases} \quad (11)$$

The stability conditions in (10) can either be a specific criterion like eigenvalue or binary stability conditions through one hot encoding. To relieve the computational burden, branch power flow, and bus voltage can be excluded in for frequency dynamics prediction. Note that DNN typically doesn't achieve 100% prediction accuracy, which could pose risks to microgrids. Hence, this paper develops a workflow that integrates full-order TDS to make the data-driven method convincing in power grids, as illustrated in Section IV.

## IV. WORKFLOW FOR SOLVING MICROGRID VIRTUAL INERTIA SCHEDULING

This section presents an efficient workflow for solving microgrid-VIS. Several strategies are introduced to facilitate the seamless integration of DNN into microgrid-VIS.

### A. General workflow

As shown in Fig. 2, the workflow for solving microgrid-VIS has three key steps: i). initialization, ii). dynamic approximation and linearization, iii). solution and validation.

- Step 1 involves initializing VIS by specifying the target system and the generic model. In this paper, the generic model is specified as microgrid-VIS in Section III. Additionally, a dynamic model for TDS is configured in ANDES [34], an open-source Python library for power system analysis and a foundation for the CURENT Large-scale Testbed (LTB) [35]. ANDES is utilized for batch dynamic data generation and validating the VIS results to ensure stability and dynamic performance.
- Step 2 focuses on generating batch data for dynamic approximation using DNN, which is then employed to linearize the original VIS model. Such linear rules extracted from simulation results, as demonstrated in [32] and [36], have been proven to be sufficient for encoding frequency dynamics. Further details on data generation, cleaning, and labeling will be introduced in Subsection IV-B.
- Step 3 involves solving the linearized VIS and validating the scheduling results through TDS performed in ANDES. If the scheduling results fail to satisfy the stability and transient performance constraints, additional corrections are needed, as detailed in Subsection IV-C.

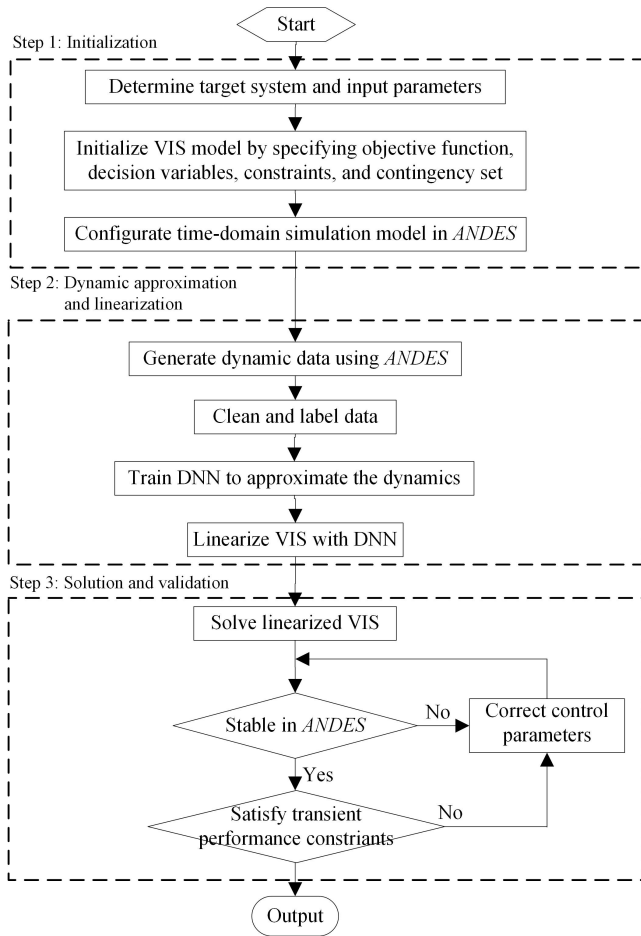


Fig. 2. Diagram of workflow for solving microgrid-VIS.

### B. Data generation, cleaning, and labeling

Given a predefined disturbance, power system TDS tools such as ANDES typically output transient trajectories of system states. These raw data must undergo cleaning and labeling before being utilized for DNN training.

1) *Data generation*: The performance of a DNN is highly dependent on the quality of the training data. When the training data adequately covers the relevant scenarios, the trained DNN will exhibit strong performance. In this paper, the raw training data, specifically TDS data, is generated using Monte Carlo Simulation based on predefined system parameters. Considering that grid topology and control structure typically do not change within the scheduling time scale, these factors are kept fixed to reduce computational complexity.

The fixed system parameters include system topology, dynamic models (such as the governor and exciter) of SGs, and dynamic models (such as voltage and current regulators) of IBRs. The variable system parameters include load conditions, contingencies, the power output of SGs and IBRs, as well as the virtual inertia and damping of IBRs. Under these assumptions, the DNN trained on the generated data adapts to these changing factors but not to fixed factors like topology and control structure. However, these fixed factors can still be accounted for by encoding the topology and control structure into the design of DNN architecture and enhancing the quality

of the training data by incorporating them into the data generation process.

Load conditions are extracted from historical data and clustered as a few representative scenarios to enhance computational efficiency. Generation output is determined based on the conventional economic dispatch model without considering dynamic constraints. To improve the efficiency of data generation, virtual inertia and damping are first sampled uniformly within the specific upper and lower boundaries. Then, region-of-interest active sampling [32] is employed to sample under marginal stability conditions.

Then, for each contingency, with fixed system parameters, and a set of changing system parameters, TDS is performed utilizing ANDES. Time-series data for frequency and power angle, and system eigenvalues before and after each contingency are recorded for further processing.

2) *Data cleaning and labeling*: The raw transient trajectories are challenging to use directly for DNN training. They are cleaned and labeled in sequence through the following steps.

- *Transform time-series data to dynamic indices*: Maximum frequency nadir and maximum RoCoF are obtained from time-series frequency data, while the maximum power angle deviation is calculated from time-series power angle data using (12) [37], [38].

$$\Delta\delta_{\max} = \max(|\delta_j(t) - \delta_k(t)|), \forall j, k \in \Omega^G, t > 0 \quad (12)$$

- *Clean unusual data*: Due to the inclusion of large disturbances such as generation trips in the contingency set, some data may deviate several orders of magnitude beyond the normal range. This could lead to singularities and pose a significant burden on DNN training. To address this, unusual maximum RoCoF, maximum frequency deviation, and maximum angle difference are transformed to a reasonable value, as shown in (13)-(15). Additionally, for each scenario, recorded eigenvalues are transformed to a single real number by keeping the maximum real part of all the eigenvalues. Real numbers with large magnitudes are also transformed to reasonable values, as shown in (16)-(17).

$$RoCoF_{\max,i} = \begin{cases} -1 & RoCoF_i < -1 \\ RoCoF_{\max,i} & -1 \leq RoCoF_i \leq 1 \\ 1 & RoCoF_i > 1 \end{cases} \quad (13)$$

$$\Delta f_{\max,i} = \begin{cases} -1 & \Delta f_{\max,i} < -1 \\ \Delta f_{\max,i} & -1 \leq \Delta f_{\max,i} \leq 1 \\ 1 & \Delta f_{\max,i} > 1 \end{cases} \quad (14)$$

$$\Delta\delta_{\max,i} = \begin{cases} \Delta\delta_{\max,i} & \Delta\delta_{\max,i} \leq 2\pi \\ 2\pi & \Delta\delta_{\max,i} > 2\pi \end{cases} \quad (15)$$

$$eig_{\max,i}^{\text{real}} = \begin{cases} 1 & eig_{\max,i}^{\text{real}} > 1 \\ eig_{\max,i}^{\text{real}} & eig_{\max,i}^{\text{real}} \leq 1 \end{cases} \quad (16)$$

where

$$eig_{\max,i}^{\text{real}} = \max[\text{real}(eig_{\text{pre}}), \text{real}(eig_{\text{post}})] \quad (17)$$



Note that the transformation thresholds in (13)-(17) can be customized, as long as they remain in proximity to the normal values defined in IEEE standards. The unusual data mapping may alter the dynamic approximation results of the DNN, but it will not affect the optimization outcomes once integrated into microgrid-VIS. This is because the mapped results still fail to meet the thresholds defined by IEEE standards, rendering them infeasible solutions within the optimization process.

- Label data: Using the cleaned data, the final training data are labeled as  $[RoCoF_{\max}, \Delta f_{\max}, eig_{\max}^{real}, \Delta \delta_{\max}]$ , where  $eig_{\max}^{real}$  quantifies the small-signal stability and  $\Delta \delta_{\max}$  quantified the large-signal transient stability. These labels align the dynamic constraints formulated in (7)-(8).

### C. TDS-based validation and correction

It is acknowledged that a DNN hardly achieves 100% prediction accuracy, especially in new testing scenarios. Such slight mismatches are critical in power systems because a minor control error can lead to severe outcomes. Therefore, TDS validation and correction are integral parts of the solution workflow.

After solving the linearized VIS, check both transient performance and stability with the implementation of VIS results in ANDES. If constraints (7)-(8) are violated after running TDS, corrections are implemented, which are categorized into the following three conditions.

- RoCoF constraint violation: Increase the virtual inertia of IBRs that are below the upper boundary with a small step size, as shown in (18). Through a few rounds of iteration, it is trivial to find the minimum  $\Delta M$  that makes TDS results satisfy RoCoF constraints.

$$M_i^{ibr'} = \begin{cases} M_i^{ibr} & M_i^{ibr} = \overline{M_i^{ibr}} \\ M_i^{ibr} + \Delta M & M_i^{ibr} < \overline{M_i^{ibr}} \end{cases} \quad (18)$$

- Frequency nadir constraints violation: Increase virtual damping using the grid search method, similar to the approach used for addressing RoCoF violation, as expressed in (19).

$$D_i^{ibr'} = \begin{cases} D_i^{ibr} & D_i^{ibr} = \overline{D_i^{ibr}} \\ D_i^{ibr} + \Delta D & D_i^{ibr} < \overline{D_i^{ibr}} \end{cases} \quad (19)$$

- Stability constraints violation: Reset virtual inertia and damping to default conservative values. The default values could be extracted from the generated batch data.

These correction methods ensure that VIS results are validated to satisfy both static and dynamic security constraints. It is important to emphasize that VIS results are generally feasible in most conditions, implying that the control parameter corrections will not be triggered. They are just backup for performance guarantee under edge scenarios.

## V. CASE STUDY

This section demonstrates microgrid-VIS in an islanded microgrid modified from the IEEE 123-bus system. Comparison studies are conducted to show the advantages of VIS with static and dynamic security constraints.

TABLE I. Cost data

Generator ID	Generation cost			Inertia cost	Damping cost
	a [\$/p.u.2]	b [\$/p.u.]	c [\$]	d [\$/p.u.]	e [\$/p.u.]
SG1	0.014	10	100	/	/
SG2	0.015	20	150	/	/
SG3	0.02	30	200	/	/
IBR1	0	0	0	3	2
IBR2	0	0	0	4	3
IBR3	0	0	0	1	1
IBR4	0	0	0	1	1
IBR5	0	0	0	2	1.5
IBR6	0	0	0	1	1
IBR7	0	0	0	1	1
IBR8	0	0	0	1	1

### A. Case overview

1) *Configuration of islanded microgrid*: Fig. 3 shows the diagram of the islanded microgrid modified from the IEEE 123-bus system. It is configured by connecting 3 SGs and 8 IBRs, such that forms a self-sufficient system when the switch nodes 149 and 150 are closed. Tab. I shows the cost data, including power generation cost, inertia cost, and damping cost. The cost coefficients  $a$ ,  $b$ , and  $c$  for IBRs are set to zero, as capital costs are not considered and there are no fuel costs for renewable energy sources. The dynamic cost coefficients  $d$  and  $e$  are set to ensure that dynamic support costs are comparable to those of conventional auxiliary services. The contingency set includes  $\pm 5\%$ ,  $\pm 10\%$  load change, and unplanned single SG trip.

As for dynamic data, SGs are equipped with governors and excitors, and their capacities are assumed to be much larger than IBRs. IBRs are controlled in VSG mode (using the REGCV1 model [39] in ANDES) with controllable virtual inertia and damping, constrained within the ranges of [0.01, 6] p.u. and [0.01, 4] p.u., respectively. The upper limits for virtual inertia and damping are defined based on SGs with the same capacity, while the lower limits are set slightly above zero to ensure basic VSG control functionality. Detailed models and parameters used in ANDES have been uploaded to the LTB website and made public to readers [40].

2) *Scheduling schemes*: Three scheduling schemes (Schemes I, II, and III) are designed as baselines for comparison to show the advantage of the proposed microgrid-VIS (Scheme IV):

- Scheme I involves the conventional economic dispatch, considering the static security constraints. Virtual inertia  $M$  and damping  $D$  of IBRs are not decision variables and are set at the upper boundary to ensure dynamic performance.
- Scheme II integrates the conventional economic dispatch, taking into account the cost of inertia and damping support, along with the static security securities. It formulates  $M$  and  $D$  as decision variables but ignores the dynamic security constraints.
- Scheme III implements VIS with static constraints, transient performance constraints, and small-signal stability constraints. It doesn't address stability issues arising from large disturbances like an unplanned SG trip.

- Scheme IV employs the proposed microgrid-VIS with comprehensive static and dynamic security constraints outlined in (6)-(8).

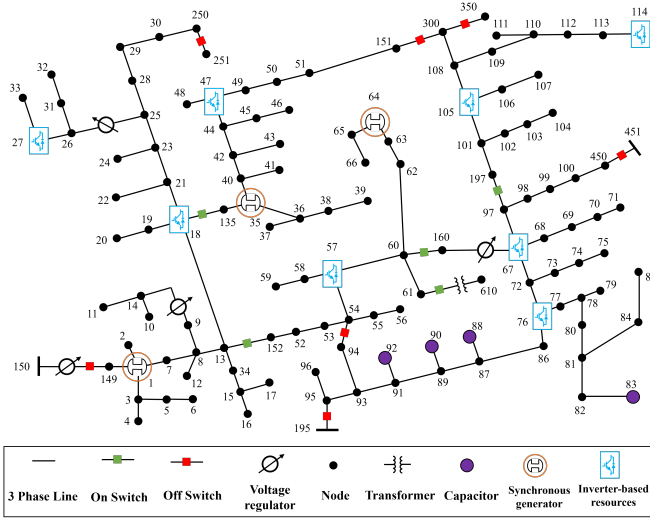


Fig. 3. Diagram of islanded microgrid modified from IEEE-123 bus distribution system.

### B. Dynamic training and approximation

Dynamic training and approximation are performed for Schemes III and IV in an environment equipped with Intel(R) Core i7-12800HX running at 2.0 GHz, 64 GB of memory, and ANDES 1.8.8.

Following the guideline in Subsection IV-B, ten thousand scenarios are randomly generated and simulated. Virtual inertia and damping are sampled uniformly using NumPy function ‘*random.uniform*’ within their upper and lower limits. After data generation, cleaning, and labeling, a fully connected neural network with one hidden layer ( $m=1$ ) containing 128 neurons ( $n=128$ ) is built in PyTorch 2.0.1 and trained to approximate the dynamics of the islanded microgrid.

### C. Solution and validation

The optimization model with one scheduling interval ( $T = 1$ ) is formulated using AMS [41] and solved with GUROBI 9.5.2. AMS is a power market simulation tool developed with Python, as an important part of CURENT’s LTB [35].

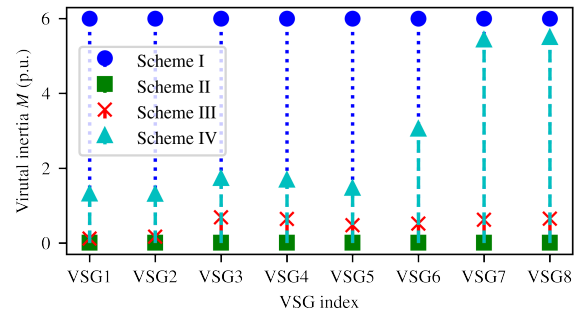
1) *Scheduling results*: Schemes I-IV yield identical scheduling results for active power generation:  $[p_{SG1}, p_{SG2}, p_{SG3}] = [17.50, 31.50, 26.75]$  MW and  $[p_{IBR1}, p_{IBR2}, p_{IBR3}, p_{IBR4}, p_{IBR5}, p_{IBR6}, p_{IBR7}, p_{IBR8}] = [7.00, 8.40, 4.90, 4.20, 6.30, 5.25, 5.60, 5.95]$  MW. However, they exhibit distinct scheduling results for virtual inertia and damping, as illustrated in Fig. 4. This difference results in varied cost results and dynamic performance under disturbance, detailed in Tab. II and summarized as follows.

- Scheme I sets  $M$  and  $D$  at the highest value conservatively to ensure dynamic performance. While it satisfies all the dynamic security constraints, it incurs the highest inertia and damping support cost.

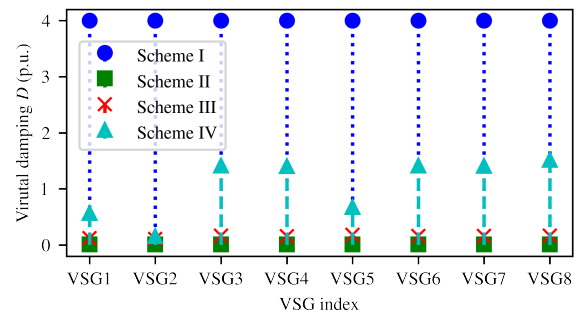
TABLE II. Scheduling results<sup>1</sup>

Item	I	II	III	IV
Total scheduling cost/\$	759.17	629.42	635.91	668.56
Inertia support cost/\$	84.00	0.14	5.09	29.60
Damping support cost/\$	46.00	0.11	1.65	9.79
RoCoF constraints	✓ ✓	× ×	✓ ×	✓ ✓
Frequency nadir constraints	✓ ✓	× ×	✓ ×	✓ ✓
Small-signal stability	✓ ✓	× ×	✓ ×	✓ ✓
Large-signal stability	✓ ✓	× ×	× ×	✓ ✓

- Scheme II has the smallest scheduling results for  $M$  and  $D$  with sole consideration of the economic aspect. This aggressive setting results in the lowest scheduling cost but violates all the dynamic security constraints.
- Scheme III exhibits  $M/D$  scheduling results slightly larger than those of Scheme II. It satisfies the transient performance constraints and small-signal stability constraints but loses stability after an unplanned SG trip.
- The  $M/D$  scheduling results of microgrid-VIS lie between Schemes I and III. In Fig. 4,  $M$  and  $D$  of IBR1, IBR2, and IBR3 and lower than other IBRs due to their high support cost. The scheduling results not only satisfy all the static and dynamic security constraints like the conservative Scheme I but strike a good tradeoff between economy and dynamic performance.



(a)



(b)

Fig. 4. Virtual inertia and damping scheduling results: (a)  $M$ , (b)  $D$ .

2) *TDS validation*: The scheduling results are further validated in ANDES. Figs. 5 and 6 present the TDS results of Schemes I-IV, visualizing the dynamic performance as

<sup>1</sup>Note: “✓” means satisfying the constraints; “×” means violating the constraints; “|” separates the results for load change and generation trip.



summarized in Tab. 2. The transient curves include frequency, RoCoF, and bus voltage. In ANDES, RoCoF is calculated numerically and measured through a low pass filter, with this paper setting the filter time constant as  $T_w = T_r = 0.3$ .

In Figs. 5 and 6, two contingencies are simulated: a 10% load increase and an unplanned trip of SG2 occurring at 5 seconds, respectively. The observations are summarized as follows:

- Implementation of Scheme I results in a maximum frequency deviation and RoCoF being 0.1 Hz and 0.078 Hz/s after load change, and 0.32 Hz and 0.2 Hz/s after the SG2 trip. These values are comfortably below the threshold of 0.6 Hz and 0.5Hz/s, attributable to the conservative settings. Moreover, unplanned SG2 trip results in larger frequency and voltage deviations than a 10% load increase.
- Implementation of Scheme II leads to microgrid diverging after both a 10% load change and the SG2 trip, thereby violating the dynamic security constraints.
- The dynamic performance of Scheme III is better than that of Scheme II. After a 10% load increase, the maximum frequency deviation and RoCoF are 0.25 Hz and 0.26 Hz/s, meeting small-signal stability constraints. However, the islanded microgrid collapses after the SG2 trip, violating the large-signal stability constraints.
- Scheme IV results in the microgrid converging to a new equilibrium after both a load change and the SG2 trip. In particular, the maximum RoCoF reaches the threshold, with the frequency nadir slightly below the threshold.

In summary, the four schemes differ in terms of virtual inertia and damping support, with the costs ranked as follows:  $C_{II}^{aux} < C_{III}^{aux} < C_{IV}^{aux} < C_I^{aux}$ . Correspondingly, their stability performance improves in line with the cost in virtual inertia and damping. This additional dynamic service cost is a distinguishing factor in the proposed framework compared to the conventional microgrid operation model. It outperforms the conventional schemes in achieving a balance between economic benefits and dynamic performance. Following a disturbance, microgrid-VIS ensures compliance with both static and dynamic security constraints.

## VI. CONCLUSION

To address the challenges arising from the decreasing physical inertia in microgrids, this paper proposes microgrid-VIS considering both the static and dynamic security constraints. Managing microgrid inertia solely from an economic standpoint can be risky, as changes to the virtual inertia and damping of IBRs can significantly alter power grid dynamics, leading to stability issues (Schemes II and III). Conversely, setting virtual inertia and damping at a high value is conservative, incurring higher opportunity costs (Scheme I), or increased investment in BESS. Microgrid-VIS offers a solution by proactively designing the inertia contributions of IBRs. This approach not only meets economic goals but also ensures the frequency profiles following significant disturbances. Furthermore, it effectively addresses the challenges associated with device-level control parameter change, thus advancing

the evolution of microgrids dominated by power electronic interfaced DERs.

This paper employs DNNs to explicitly express and linearize the dynamic security constraints, with TDS used to correct and validate the scheduling results. Because DNN is unexplainable, future work will dive into deriving model-based criteria to make the formulation trackable and easy to understand. In addition, the extension of VIS to multi-components with active inertia support capability and multi-energy systems will be explored.

## ACKNOWLEDGMENT

The authors would like to thank the financial support in part from the US DOD ESTCP program under grant number EW20-5331 to complete this research work.

## REFERENCES

- [1] B. She, F. Li, H. Cui, J. Zhang, and R. Bo, "Fusion of microgrid control with model-free reinforcement learning: review and vision," *IEEE Transactions on Smart Grid*, 2022.
- [2] L. Wang, Y. Qin, Z. Tang, and P. Zhang, "Software-defined microgrid control: The genesis of decoupled cyber-physical microgrids," *IEEE Open Access Journal of Power and Energy*, vol. 7, pp. 173–182, 2020.
- [3] B. She, F. Li, H. Cui, H. Shuai, O. Oboreh-Snapps, R. Bo, N. Praisuwana, J. Wang, and L. M. Tolbert, "Inverter PQ control with trajectory tracking capability for microgrids based on physics-informed reinforcement learning," *IEEE Transactions on Smart Grid*, 2023.
- [4] D. Pullaguram, R. Madani, T. Altun, and A. Davoudi, "Small-signal stability-constrained optimal power flow for inverter dominant autonomous microgrids," *IEEE Transactions on Industrial Electronics*, vol. 69, no. 7, pp. 7318–7328, 2021.
- [5] G. Magdy, H. Ali, and D. Xu, "Effective control of smart hybrid power systems: Cooperation of robust LFC and virtual inertia control systems," *CSEE Journal of Power and Energy Systems*, vol. 8, no. 6, pp. 1583–1593, 2021.
- [6] A. Fawzy, A. Bakeer, G. Magdy, I. E. Atawi, and M. Roshdy, "Adaptive virtual inertia-damping system based on model predictive control for low-inertia microgrids," *IEEE Access*, vol. 9, pp. 109 718–109 731, 2021.
- [7] M. Li, W. Huang, N. Tai, L. Yang, D. Duan, and Z. Ma, "A dual-adaptivity inertia control strategy for virtual synchronous generator," *IEEE Transactions on Power Systems*, vol. 35, no. 1, pp. 594–604, 2019.
- [8] H. Xu, C. Yu, C. Liu, Q. Wang, and X. Zhang, "An improved virtual inertia algorithm of virtual synchronous generator," *Journal of Modern Power Systems and Clean Energy*, vol. 8, no. 2, pp. 377–386, 2019.
- [9] U. Markovic, Z. Chu, P. Aristidou, and G. Hug, "LQR-based adaptive virtual synchronous machine for power systems with high inverter penetration," *IEEE Transactions on Sustainable Energy*, vol. 10, no. 3, pp. 1501–1512, 2018.
- [10] J. Pahasa, P. Potejana, and I. Ngamroo, "MPC-based virtual energy storage system using PV and air conditioner to emulate virtual inertia and frequency regulation of the low-inertia microgrid," *IEEE Access*, vol. 10, pp. 133 708–133 719, 2022.
- [11] Y. Su, H. Li, Y. Cui, S. You, Y. Ma, J. Wang, and Y. Liu, "An adaptive PV frequency control strategy based on real-time inertia estimation," *IEEE Transactions on Smart Grid*, vol. 12, no. 3, pp. 2355–2364, 2020.
- [12] D. Curto, S. Favuzza, V. Franzitta, A. Guercio, M. A. N. Navia, E. Telaretti, and G. Zizzo, "Grid stability improvement using synthetic inertia by battery energy storage systems in small islands," *Energy*, vol. 254, p. 124456, 2022.
- [13] O. Oboreh-Snapps, B. She, S. Fahad, H. Chen, J. Kimball, F. Li, H. Cui, and R. Bo, "Virtual synchronous generator control using twin delayed deep deterministic policy gradient method," *IEEE Transactions on Energy Conversion*, 2023.
- [14] J. Liu, Y. Zhang, A. J. Conejo, and F. Qiu, "Ensuring transient stability with guaranteed region of attraction in dc microgrids," *IEEE Transactions on Power Systems*, vol. 38, no. 1, pp. 681–691, 2022.
- [15] Y. Chen, S. M. Mazhari, C. Chung, and S. O. Faried, "A preventive dispatching method for high wind power-integrated electrical systems considering probabilistic transient stability constraints," *IEEE Open Access Journal of Power and Energy*, vol. 8, pp. 472–483, 2021.

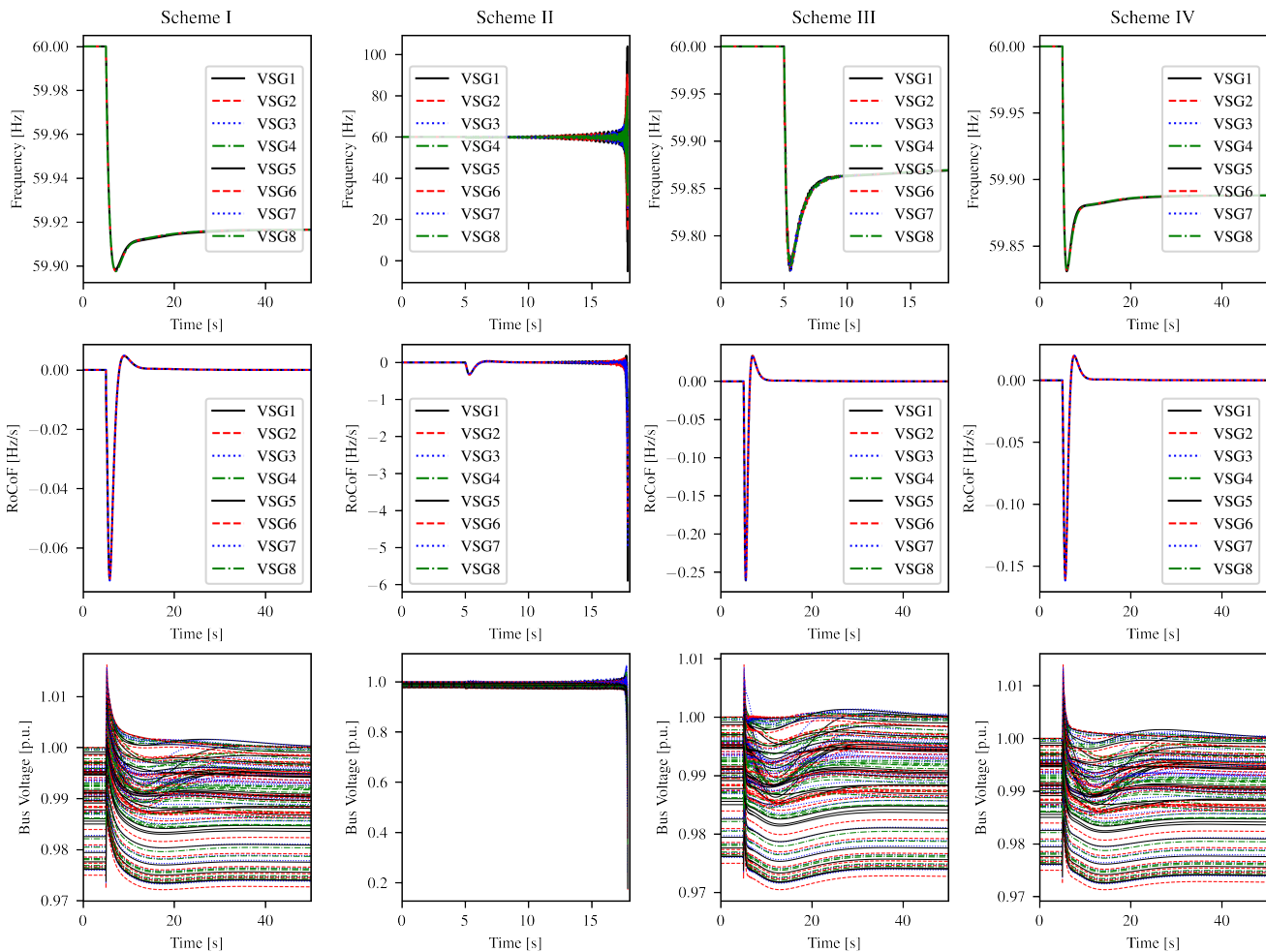


Fig. 5. Dynamic performance of microgrid under 10% load increase.

- [16] F. Arredondo, P. Ledesma, E. D. Castronuovo, and M. Aghahassani, "Stability improvement of a transmission grid with high share of renewable energy using TSCOPF and inertia emulation," *IEEE Transactions on Power Systems*, vol. 37, no. 4, pp. 3230–3237, 2020.
- [17] S. Nikkiah, M.-A. Nasr, and A. Rabiee, "A stochastic voltage stability constrained ems for isolated microgrids in the presence of pevs using a coordinated uc-opf framework," *IEEE Transactions on Industrial Electronics*, vol. 68, no. 5, pp. 4046–4055, 2020.
- [18] H. Jing, J. Kweon, Y. Li, and V. Monga, "Enhancing dynamic resilience of networked microgrids with a high penetration of power-electronic-interfaced DERs," in *2022 IEEE Power & Energy Society General Meeting (PESGM)*. IEEE, 2022, pp. 1–5.
- [19] P. Pareek and H. D. Nguyen, "A convexification approach for small-signal stability constrained optimal power flow," *IEEE Transactions on Control of Network Systems*, vol. 8, no. 4, pp. 1930–1941, 2021.
- [20] B. K. Poolla, S. Bolognani, N. Li, and F. Dörfler, "A market mechanism for virtual inertia," *IEEE Transactions on Smart Grid*, vol. 11, no. 4, pp. 3570–3579, 2020.
- [21] J. Fang, H. Li, Y. Tang, and F. Blaabjerg, "On the inertia of future more-electronics power systems," *IEEE Journal of Emerging and Selected Topics in Power Electronics*, vol. 7, no. 4, pp. 2130–2146, 2018.
- [22] B. She, F. Li, H. Cui, J. Wang, Q. Zhang, and R. Bo, "Virtual inertia scheduling (VIS) for real-time economic dispatch of IBRs-penetrated power systems," *IEEE Transactions on Sustainable Energy*, 2023.
- [23] S. Lei, Y. Zhang, M. Shahidehpour, Y. Hou, M. Panteli, X. Chen, N. Y. Aydin, L. Liang, C. Wang, C. Wang *et al.*, "Guest editorial: Operational and structural resilience of power grids with high penetration of renewables," *IET Renewable Power Generation*, vol. 18, no. 7, pp. 1055–1059, 2024.
- [24] D. G. Photovoltaics and E. Storage, "Ieee standard for interconnection and interoperability of distributed energy resources with associated electric power systems interfaces," *IEEE std*, vol. 1547, no. 1547, p. 2018, 2018.
- [25] N. Hatzigrygiou, J. Milanovic, C. Rahmann, V. Ajarapu, C. Canizares, I. Erlich, D. Hill, I. Hiskens, I. Kamwa, B. Pal *et al.*, "Definition and classification of power system stability-revisited & extended," *IEEE Transactions on Power Systems*, vol. 36, no. 4, pp. 3271–3281, 2020.
- [26] U. Tamrakar, D. A. Copp, T. Nguyen, T. M. Hansen, and R. Tonkoski, "Optimization-based fast-frequency estimation and control of low-inertia microgrids," *IEEE Transactions on Energy Conversion*, vol. 36, no. 2, pp. 1459–1468, 2020.
- [27] L. Bai, J. Wang, C. Wang, C. Chen, and F. Li, "Distribution locational marginal pricing (dlmp) for congestion management and voltage support," *IEEE Transactions on Power Systems*, vol. 33, no. 4, pp. 4061–4073, 2017.
- [28] H.-G. Yeh, D. F. Gayme, and S. H. Low, "Adaptive var control for distribution circuits with photovoltaic generators," *IEEE Transactions on Power Systems*, vol. 27, no. 3, pp. 1656–1663, 2012.
- [29] J. Wang, F. Fan, Y. Song, Y. Hou, and D. J. Hill, "Stability constrained optimal operation of inverter-dominant microgrids: A two stage robust optimization framework," *IEEE Transactions on Sustainable Energy*, 2024.
- [30] B. She, J. Liu, F. Qiu, H. Cui, N. Praisuwan, J. Wang, L. M. Tolbert, and F. Li, "Systematic controller design for inverter-based microgrids with certified large-signal stability and domain of attraction," *IEEE Transactions on Smart Grid*, 2023.
- [31] Y. Zhang, C. Chen, G. Liu, T. Hong, and F. Qiu, "Approximating trajectory constraints with machine learning–microgrid islanding with frequency constraints," *IEEE Transactions on Power Systems*, vol. 36, no. 2, pp. 1239–1249, 2020.
- [32] Y. Zhang, H. Cui, J. Liu, F. Qiu, T. Hong, R. Yao, and F. Li, "Encoding frequency constraints in preventive unit commitment using deep learning

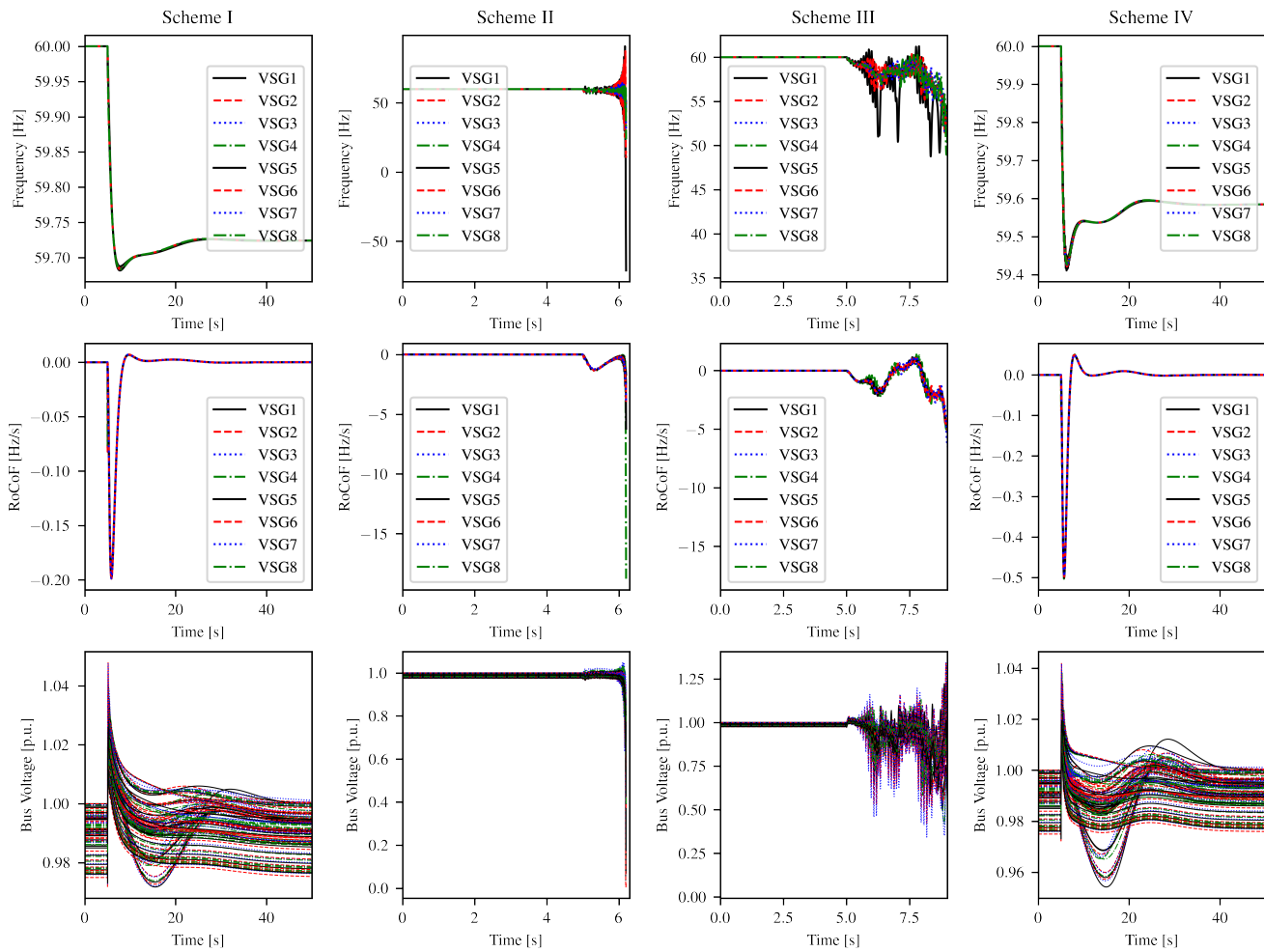


Fig. 6. Dynamic performance of microgrid under unplanned SG2 trip.

with region-of-interest active sampling,” *IEEE Transactions on Power Systems*, vol. 37, no. 3, pp. 1942–1955, 2021.

[33] B. Jiang, C. Guo, and Z. Chen, “Frequency constrained unit commitment considering reserve provision of wind power,” *Applied Energy*, vol. 361, p. 122898, 2024.

[34] H. Cui, F. Li, and K. Tomsovic, “Hybrid symbolic-numeric framework for power system modeling and analysis,” *IEEE Transactions on Power Systems*, vol. 36, no. 2, pp. 1373–1384, 2020.

[35] F. Li, K. Tomsovic, and H. Cui, “A large-scale testbed as a virtual power grid: For closed-loop controls in research and testing,” *IEEE Power and Energy Magazine*, vol. 18, no. 2, pp. 60–68, 2020.

[36] J. Zhang, Z. Chen, N. Zhang, and X. Zhang, “Frequency-constrained unit commitments with linear rules extracted from simulation results considering regulations from battery storage,” *Journal of Modern Power Systems and Clean Energy*, 2023.

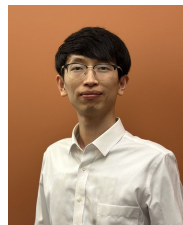
[37] S. M. Mazhari, B. Khorramdel, C. Chung, I. Kamwa, and D. Novosel, “A simulation-based classification approach for online prediction of generator dynamic behavior under multiple large disturbances,” *IEEE Transactions on Power Systems*, vol. 36, no. 2, pp. 1217–1228, 2020.

[38] L. Zhu, D. J. Hill, and C. Lu, “Semi-supervised ensemble learning framework for accelerating power system transient stability knowledge base generation,” *IEEE Transactions on Power Systems*, vol. 37, no. 3, pp. 2441–2454, 2021.

[39] H. Cui, “Andes manual,” 2024. [Online]. Available: <https://docs.andes.app/en/stable/groupdoc/Gen.html#regcv1>

[40] B. She, F. Li, and J. Wang. (2023) Case file: Virtual inertia scheduling (VIS) for microgrids with static and dynamic security constraints. [Online]. Available: <https://ltb.curent.org/showcase/microvis/>

[41] J. Wang, “Ams manual,” 2023. [Online]. Available: <https://ltb.readthedocs.io/projects/ams/en/latest/>



**Buxin She** (Member, IEEE) received the B.S.E.E and M.S.E.E degrees from Tianjin University, China in 2017 and 2019, and the Ph.D. degree from the University of Tennessee, Knoxville in 2023, all in electrical engineering. He is currently a research engineer at Pacific Northwest National Laboratory (PNNL). He served as a student guest editor of IET-RPG. He was an outstanding reviewer of IEEE OAJPE (2020) and MPCE (2022 and 2023). His research interests include microgrid operation and control, machine learning in power systems, distribution system operation and plan, and power grid resilience.



**Fangxing Li** (Fellow, IEEE) is also known as Fran Li. He received the B.S.E.E. and M.S.E.E. degrees from Southeast University, Nanjing, China, in 1994 and 1997, respectively, and the Ph.D. degree from Virginia Tech, Blacksburg, VA, USA, in 2001. Currently, he is the John W. Fisher Professor in electrical engineering at the University of Tennessee, Knoxville, TN, USA. He has been the Director of CURENT since 2024. His research interests include resilience, artificial intelligence in power, distributed energy resources (DERs) and microgrid, and electricity markets.

From 2020 to 2021, he served as the Chair of IEEE PES Power System Operation, Planning and Economics (PSOPE) Committee. Currently, he is serving as the Chair of IEEE WG on Machine Learning for Power Systems and the Editor-In-Chief of *IEEE Open Access Journal of Power and Energy (OAJPE)*.

Prof. Li has received numerous awards and honors including R&D 100 Award in 2020, IEEE PES Technical Committee Prize Paper award twice in 2019 and 2024, 6 best or prize paper awards at international journals, and 7 best papers/posters at international conferences.



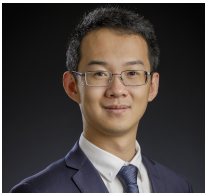
**Rui Bo** (Senior Member, IEEE) received the BSEE and MSEE degrees in electric power engineering from Southeast University (China) in 2000 and 2003, respectively, and received the Ph.D. degree in electrical engineering from the University of Tennessee, Knoxville (UTK) in 2009. He is currently an Associate Professor of the Electrical and Computer Engineering Department with the Missouri University of Science and Technology (formerly the University of Missouri-Rolla). He worked as a Principal Engineer and Project Manager at Midcontinent Independent

System Operator (MISO) from 2009 to 2017. His research interests include computation, optimization and economics in power system operation and planning, high performance computing, electricity market simulation, evaluation, and design.



**Jinning Wang** (Graduate Student Member, IEEE) received the B.S. and M.S. degrees in electrical engineering from the Taiyuan University of Technology, Taiyuan, China, in 2017 and 2020, respectively. He is currently pursuing a Ph.D. degree in electrical engineering with the University of Tennessee, Knoxville, TN, USA. His research interests include data mining, scientific computation, and power system simulation. He is the author of AMS, a power system dispatch simulator, which is a key component of the CURENT Large-scale Testbed. He also

curates the list Popular Open Source Libraries for Power System Analysis.



**Hantao Cui** (Senior Member, IEEE) received the B.S. and M.S. degrees from Southeast University, China in 2011 and 2013, and the Ph.D. degree from the University of Tennessee, Knoxville in 2018, all in electrical engineering. He is currently an Associate Professor with the Department of Electrical and Computer Engineering, North Carolina State University. His research interests include power system modeling, simulation, and high-performance computing.



**Xiaofei Wang** (Member, IEEE) received the B.S.E.E. degree from North China Electric Power University in 2014, China, the M.S.E.E. degree from Wuhan University, China, in 2017, and the Ph.D. degree from The University of Tennessee, Knoxville, TN, USA, in 2023. He is currently a Postdoctoral Researcher with National Renewable Energy Laboratory. His research interests include the electricity market, power system resilience, and distributed energy resource integration.